The Astronomical Journal, 145:7 (15pp), 2013 January doi:10.1088/0004-6256/145/1/7

NGC 6811: AN INTERMEDIATE-AGE CLUSTER IN THE *KEPLER* FIELD

Kenneth Janes[1], Sydney A. Barnes[2,4], Søren Meibom[3], and Sadia Hoq[1]
[1] Astronomy Department, Boston University, Boston, MA 02215, USA
[2] Space Science Institute, Boulder, CO 80301, USA
[3] Center for Astrophysics, 60 Garden St., Cambridge, MA 02138, USA
Received 2012 August 21; accepted 2012 October 21; published 2012 December 6

ABSTRACT

NGC 6811 is one of the four open clusters located in the *Kepler* spacecraft field of view. We obtained *UBVRI* photometry of the cluster on six nights (four of them photometric) with the 1.08 m Hall and 1.83 m Perkins telescopes at Lowell Observatory. The mean photometric precision ranges from better than 0.01 mag in the V, $B-V$, $V-R$, and $V-I$ indices among stars brighter than magnitude 15 to about 0.05 mag for $U-B$ at magnitude 18. We followed a Bayesian statistical approach using the Markov Chain Monte Carlo algorithm to determine the cluster reddening, distance, age, and iron content from a maximum-likelihood fit to stellar isochrones. Using the Yale–Yonsei isochrones, we derived $E(B-V) = 0.066 \pm 0.025$, $(m-M)_V = 10.13 \pm 0.19$, age $= 1.06 \pm 0.19$ Gyr, and $Z = 0.012 \pm 0.004$ ([Fe/H] $= -0.18$); with the Padova isochrones, we found $E(B-V) = 0.081 \pm 0.015$, $(m-M)_V = 10.31 \pm 0.11$, age $= 0.94 \pm 0.08$ Gyr, and $Z = 0.012 \pm 0.002$ ([Fe/H] $= -0.20$). The uncertainties include possible errors in the photometric zero points of ± 0.01 mag, but do not include uncertainties in the models. Taking into account the differences between the two sets of models, we find the best estimate for the cluster parameters to be $E(B-V) = 0.074 \pm 0.024$, $(m-M)_V = 10.22 \pm 0.18$, age $= 1.00 \pm 0.17$ Gyr, and $Z = 0.012 \pm 0.004$ ([Fe/H] $= -0.19$).

Key words: Hertzsprung-Russell and C-M diagrams – methods: data analysis – open clusters and associations: individual (NGC 6811)

Online-only material: machine-readable and VO tables

1. INTRODUCTION

The range in ages of the four open clusters located within the field of view of the *Kepler* spacecraft (Borucki et al. 2011) spans the history of the galactic disk. This circumstance makes them ideal targets for probing the age–rotation–period relation of main-sequence stars. The *Kepler* Cluster Study (Meibom et al. 2011b) will make use of *Kepler*'s exquisite photometric precision to probe the rotation periods of stars in these four clusters by tracking the minute variations as spots and faculae pass across their visible surfaces (see, e.g., Meibom et al. 2011a). The two older clusters in the *Kepler* field, NGC 6819 and NGC 6791, have been extensively studied, but the two younger ones, NGC 6866 and NGC 6811, had been somewhat ignored until recently. This paper is a report of a photometric study of NGC 6811, in support of the *Kepler* Cluster Study.

There have been only a few photometric studies of NGC 6811. Since the Lindoff (1972) photographic survey, Barkhatova et al. (1978), as quoted in the open cluster database WEBDA at http://univie.ac.at/webda, presented photometry of the cluster, Glushkova et al. (1999) performed a radial velocity and photoelectric *UBVRI* study, finding a distance of 1040 pc and an age of 7×10^8 years, and there have been two recent preliminary reports of NGC 6811 color–magnitude diagrams (CMDs; Mills et al. 2004; Majaess et al. 2011). The cluster is known to contain δ-Scuti variables, and there have been several variability studies, including Rose & Hintz (2007), Luo et al. (2009), and Creevey et al. (2011). Sanders (1971) found 97 cluster members brighter than magnitude ~14 from a proper motion study. Radial velocity investigations include Mermilliod & Mayor (1990), who derived a mean velocity of $V_R = 7.28\,\mathrm{km\,s^{-1}}$ (three stars). Frinchaboy & Majewski (2008) did a combined radial velocity and proper motion study, finding a radial velocity, $V_R = 6.03 \pm 0.30\,\mathrm{km\,s^{-1}}$ (seven stars), and proper motion, $\mu_\alpha \cos(\delta) = -5.31 \pm 0.67\,\mathrm{mas\,yr^{-1}}$, $\mu_\delta = -8.13 \pm 0.64\,\mathrm{mas\,yr^{-1}}$.

Hekker et al. (2011) have done a preliminary asteroseismic analysis of red giant stars in three of the *Kepler* clusters. They find that stellar mass has a significant influence on the asteroseismic quantities, but that metallicity has little or no effect. They did, however, note that NGC 6811 might have a metallicity significantly lower than that of the Sun. Also of relevance to NGC 6811 are two other *Kepler* asteroseismic studies of a large number of red giants in the *Kepler* field (Huber et al. 2010; Kallinger et al. 2010).

Because the cluster is located in the *Kepler* field of view, it has the potential to be a key resource for studies of asteroseismology, stellar rotations, and other astrophysical investigations using the *Kepler* data archive. For that reason, we undertook an extensive photometric study of the cluster to determine the cluster reddening, distance, age, and metallicity.

In Section 2 we discuss the observations and photometric reduction of the cluster data. Section 3 describes the cluster CMD and structural properties, Section 4 is an analysis of its reddening, distance, composition, and age, and Section 5 consists of a discussion and summary of the results.

2. THE PHOTOMETRIC PROGRAM

We obtained CCD images of NGC 6811 on several occasions (Table 1), using the Hall and Perkins telescopes at Lowell Observatory. Conditions were photometric on four of the six nights, and we imaged extensive sequences of Landolt (2009)

[4] Mercator Guest Professor, University of Potsdam, and Leibniz Institute for Astrophysics, Germany.

Table 1
Observing Record

UT Date	Telescope	Detector	Filters	No. of Stds.
2005 Sep 30	Hall 1.2 m	SITe CCD	B, V, I	52,38,36
2005 Oct 2	Hall 1.2 m	SITe CCD	B	None
2009 Sep 21	Perkins 1.8 m	Fairchild CCD	B, V, R, I	93,101,96,96
2010 Sep 17	Hall 1.2 m	e2v CCD	U, B, V	150,129, 137
2010 Sep 18	Hall 1.2 m	e2v CCD	U, B, V	181, 188, 208
2011 Jun 27	Perkins 1.8 m	e2v CCD	B, V	None

standard stars over a wide range of airmass on each night. On the night of 2005 October 2 (UT), the sky conditions were non-photometric; as we show in the following, we used local standards in the cluster to generate the transformation coefficients for that night. Finally, on the night of 2011 June 27 (UT), we obtained long B and V exposures of the cluster with local standards to transform the photometry from this night as well. Figure 1 illustrates the placement of the fields for the four observing seasons; the circle represents the 1σ radius of the cluster, as defined by Equation (7) (see also Table 7).

We did our initial processing of the images (bias subtraction and flat-field correction) using standard IRAF[5] functions. We used the SPS program (Janes & Heasley 1993) a stellar photometry software package for point-spread-function-fitting photometry of all images, and transformed the photometry to the *UBVRI* colors following procedures similar to those in Janes & Hoq (2011).

For the B and V photometry, we have both standard star and cluster images from all four photometric nights. For the non-photometric nights, we have B cluster images only on the night of 2005 October 2, and both B and V images on 2011 June 27. We have U and I data for two nights each and R photometry on one night. We used observations of the Landolt (2009) standard stars to derive photometric transformations. For V, $B-V$, and on some nights $U-B$, we derived coefficients of the form

$$v = V + \alpha_{bv}(B - V) + k_v X + C_{bv}, \quad (1a)$$

$$b = V + \alpha_b(B - V) + k_b X + k'_b X(B - V) + C_b, \quad (1b)$$

$$u = V + (B - V) + \alpha_{ub}(U - B) + k_u X + k'_u X(U - B) + C_{ub}; \quad (1c)$$

for V, $V-R$ the transformations are

$$v = V + \alpha_{vr}(V - R) + k_v X + C_{vr}, \quad (2a)$$

$$r = V + \alpha_r(V - R) + k_r X + C_r; \quad (2b)$$

and the V, $V-I$ coefficients are

$$v = V + \alpha_{vi}(V - I) + k_v X + C_{vi}, \quad (3a)$$

$$i = V + \alpha_i(V - I) + k_i X + C_i. \quad (3b)$$

Because we used several combinations of telescopes and detectors as well as different selections of standards, we transformed the photometry as four independent data sets and combined the results. For the night of 2005 October 2, we used preliminary magnitudes and colors in the cluster based on the photometry from the night of 2005 September 30 as local standards, and then merged the transformed photometry from 2005 September 30 and 2005 October 2 and treated the results as a single night. We transformed the two nights in 2010 September as a single data set, but with separate extinction coefficients and zero points. Finally, we used the combined results for all the other nights for local standards to calculate coefficients for the night of 2011 June 27. For this last night, we stacked three 5 minute V and three 10 minute B images for the photometry to reach as faint a limiting magnitude as possible. Table 2 shows the standard deviations of the differences between the calculated and standard values of the Landolt standards.

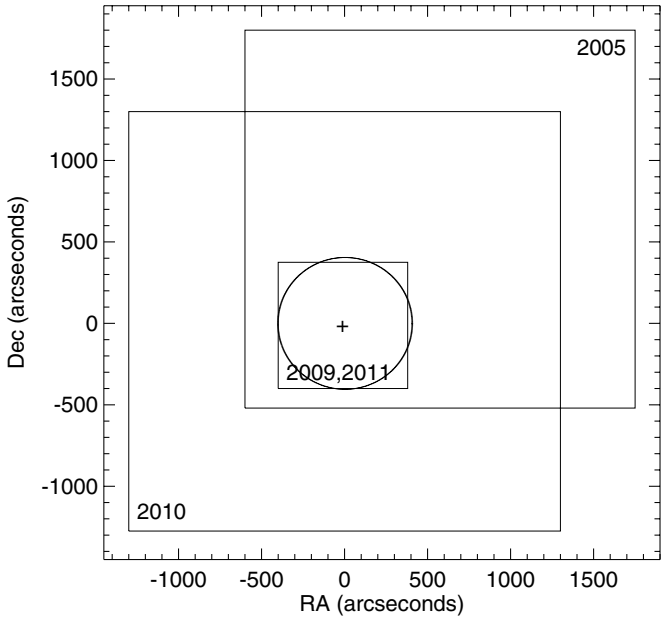

Figure 1. Locations of the fields observed in the four seasons of this project (see Table 1). The circle represents the 1σ cluster angular size as defined by Equation (7).

Although the errors of most of the transformation coefficients are less than 0.01 mag, the calculated uncertainties in the $U-B$ coefficients are between 0.01 and 0.02 mag. As a test, we tried reducing the two 2010 September nights for which we have U photometry separately. The residuals for the independent fits to the two nights are consistent with one another and with the combined solution, and there are no indications in the data that higher order color terms or piecewise solutions would make a better solution. We also searched for correlations between the $U-B$ errors and X or Y positions on the frames, airmass, $B-V$ and $U-B$ colors, frame number, Landolt field number, night, and UT, and we found no indication of any correlations.

Because the spectral sensitivity of a typical CCD detector declines toward the violet, whereas the sensitivity of a typical photomultiplier tube (on which the Landolt (2009) standard star values are based) increases toward the violet, it is possible that subtle differences in the violet spectra of stars with unusual characteristics (e.g., reddening, gravity, or metallicity) could alter the effective wavelength of the U band in such stars. Nevertheless, since we observed a total of 75 standard stars on the two nights (70 of them on both nights), we conclude that the transformation coefficients are well determined within the errors.

As mentioned above, we transformed the NGC 6811 frames from the 2005, 2009, and 2010 nights as three independent data sets and then combined the three sets. After using these

[5] IRAF is distributed by NOAO, operated by AURA under a cooperative agreement with the NSF.

Table 2
Standard Deviations of Fits to Standard Stars

	2005 September/October		2009 September	2010 September	
	2005 September 30	2005 October 2	2009 September 21	2010 September 17	2010 September 18
Equation (1a):					
Standard deviation	0.0167	...	0.0183	0.0235	
No. of standards	37	...	102	137	208
Equation (1b):					
Standard deviation	0.0172	0.0005	0.0246	0.0294	
No. of standards	51	11464	96	129	184
Equation (1c):					
Standard deviation	...	...	...	0.0620	
No. of standards	...	...	...	107	170
Equation (2a):					
Standard deviation	...	...	0.0182	...	...
No. of standards	...	...	102	...	...
Equation (2b):					
Standard deviation	...	...	0.0202	...	...
No. of standards	...	...	96	...	...
Equation (3a):					
Standard deviation	0.0171		0.0183	...	...
No. of standards	37		102	...	...
Equation (3b):					
Standard deviation	0.0206		0.0195	...	...
No. of standards	35		96	...	...

Table 3
Photometric Catalog

Star	X	Y	V	$B-V$	$U-B$	$V-R$	$V-I$	N_U	N_B	N_V	N_R	N_I
1	−1287.95	−1156.60	14.201 ± 0.032	0.483 ± 0.046	...	...	...	0	3	3	0	0
2	−1287.80	311.06	16.679 ± 0.026	1.212 ± 0.049	...	...	...	0	3	3	0	0
3	−1286.02	265.61	16.324 ± 0.021	0.862 ± 0.035	...	...	...	0	3	3	0	0
4	−1285.08	−925.79	16.648 ± 0.056	0.845 ± 0.093	...	...	...	0	3	3	0	0
5	−1283.88	−129.53	16.879 ± 0.028	0.972 ± 0.047	...	...	...	0	6	4	0	0

(This table is available in its entirety in machine-readable and Virtual Observatory (VO) forms in the online journal. A portion is shown here for guidance regarding its form and content.)

measurements to calculate transformation coefficients for the night of 2011 June 27, we merged those results into the other three data sets with appropriate weighting. In 2005 and 2010 (the Hall telescope observations) we observed a 2×2 mosaic of fields around the cluster, although because of a pointing mistake in the 2005 season, the SW quadrant was actually centered on the cluster and the other quadrants were correspondingly offset; the NE quadrant likely contains few, if any, cluster stars.

For matching stars, we used stars from the *Kepler* Input Catalog (KIC; Brown et al. 2011) to transform the individual images to a common coordinate system, centered on the nominal cluster center at R.A. $= 19^{\rm h}37^{\rm m}17\overset{\rm s}{.}0$, decl. $= 46^\circ 23' 18''$. We considered stars within 0.5 arcsec of the same position on different frames to be the same star. In cases of overlapping star images (i.e., when a star on one frame was within 0.5 arcsec of two stars on another frame), we rejected the star, irrespective of the magnitude differences of the stars on the second frame. The calculated positions for 10,674 stars in the NGC 6811 field are given in Table 3. Column 1 of the catalog contains star numbers and Columns 2 and 3 are the $X = \alpha \cos(\delta)$ and $Y = \delta$ positions, both in units of seconds of arc relative to the cluster center. The remaining columns of the catalog contain the V magnitudes and errors, $B-V$, $U-B$, $V-R$, and $V-I$ color indices and their errors and the numbers of measurements in each filter.

In merging the data for the four data sets, we accepted only stars with at least three measurements in the V filter and for which the errors in the calculated average values of the V magnitude and at least one color index are less than 0.1 mag. The errors quoted in Table 3 represent the standard deviations of the values for each index, except that for stars measured in a particular index on fewer than three frames, the error quoted is the average of the errors of the individual measurements as calculated in the SPS program.

Because we have included observations from two telescopes at several different times, the photometric errors and limiting magnitudes vary with position in the field. The catalog (Table 3) is reasonably complete to at least magnitude $V = 20$ except for a small zone near the south and west edges. In the central region, defined by the 13.3 × 13.3 arcmin field of the Perkins telescope, the limiting magnitude is close to $V = 22$. Because of the spatial variation of the depth of the photometry across the field, it would not be advisable to use the present photometry for population studies.

The mean photometric errors as a function of magnitude are summarized in Table 4. For the B and V photometry, the mean V and $B-V$ differences between each of the four data sets and the combined data are less than 0.01 mag. The mean of the $V-I$ differences between the two nights of I photometry is also less than 0.01. We reduced the two nights of U photometry (2010 September 17 and 2010 September 18) together, but as a test, we reduced them separately and compared them; the mean of the $U-B$ differences between the two nights is 0.019 mag.

Table 4
NGC 6811—Mean Photometric Errors by Magnitude

Magnitude Range	σ_V	σ_{B-V}	σ_{U-B}	σ_{V-R}	σ_{V-I}
<12	0.008	0.010	0.012	0.003	0.004
12–13	0.008	0.010	0.010	0.002	0.007
13–14	0.009	0.010	0.012	0.002	0.008
14–15	0.009	0.010	0.013	0.002	0.009
15–16	0.009	0.011	0.016	0.003	0.007
16–17	0.012	0.015	0.026	0.006	0.009
17–18	0.016	0.024	0.046	0.008	0.014
18–19	0.022	0.033	0.066	0.015	0.020
19–20	0.025	0.038	0.059	0.028	0.031
20–21	0.033	0.034	...	0.049	0.054
21–22	0.042	0.058	...	...	0.069

Table 5
Differences Between Glushkova et al. (1999) and This Work

Index	Mean	rms	n
V	0.003	0.031	92
$B-V$	−0.006	0.026	93
$U-B$	−0.040	0.060	91

Therefore the photometry in our final catalog is self-consistent within 0.01 mag.

A comparison of 93 stars in common with the Glushkova et al. (1999) *UBV* CCD photometry of the cluster (obtained from the WEBDA) shows that the mean differences between the V and $B-V$ indices are essentially zero, although there is an offset between the $(U-B)$ colors (see Table 5). The rms differences are within reasonable limits as the table shows.

We also compared our photometry of NGC 6811 with the KIC photometry (Brown et al. 2011), transformed from the *Kepler* g and r colors to $B-V$ and $V-I$ using $g-r$ to $B-V$ and $V-I$ relations. Several sets of transformation relations have been derived, including those by Jester et al. (2005) and Ivezić et al. (2007). Figure 2 shows a comparison of the present V magnitudes versus the derived V magnitudes from the KIC photometry using the Jester et al. (2005) relations. This figure is derived from photometry of the central region, which includes the deepest exposures. While overall, the V magnitudes are close, at the faint end there is a large offset in the magnitudes. The sense of the offset is such that for stars which we measure as being between magnitudes 20 and 21, the KIC magnitudes have nearly the same value near magnitude 20. The faintest stars in our catalog (Table 3) are about one magnitude fainter than the faintest stars in the KIC. Figure 2 suggests that there is a progressively larger V magnitude error toward the faintest stars in the KIC.

Table 6 is a comparison of the stars brighter than magnitude 16 in the present photometry with several transformations of the KIC *griz* photometry. In addition to the *griz* to *BVI* transformations developed by Jester et al. (2005) and Ivezić et al. (2007) mentioned above, we have developed a transformation of the KIC photometry, using the Stetson et al. (2003) *BVI* photometry of NGC 6791—located in the *Kepler* field—as a calibration source. We used the same formulation as Jester et al. (2005) to derive the following relations for 301 stars brighter than magnitude 17 in common to the KIC and the NGC 6791 photometry:

$$V = g - (0.528 \pm 0.010) \times (g - r) - (0.091 \pm 0.008), \quad (4a)$$

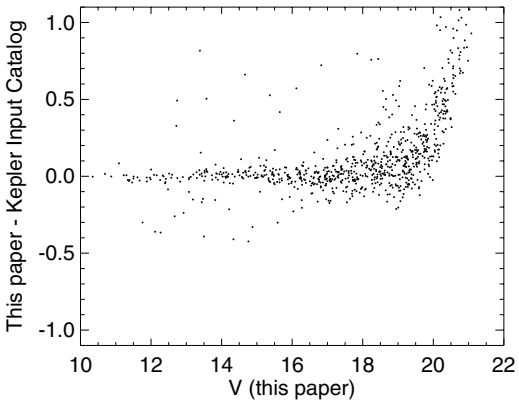

Figure 2. Comparison of V magnitudes from the present photometry with the KIC photometry, transformed to the BV system using coefficients from Jester et al. (2005). Stars from the central region only are included. The faintest KIC magnitudes are calculated to be about $V = 20$, whereas the same stars in the present photometry appear to be fainter than $V = 21$.

$$(B - V) = (1.024 \pm 0.009) \times (g - r) + 0.170 \pm 0.007), \quad (4b)$$

$$(V - I) = (2.276 \pm 0.022) \times (r - i) + (0.419 \pm 0.007). \quad (4c)$$

Although NGC 6791 is unusually metal-rich, most of the stars brighter than the 17th magnitude in the NGC 6791 field are *not* cluster members, but ordinary field stars. The rms differences between the Stetson et al. (2003) photometry and the transformed KIC values are ±0.046, ±0.040, and ±0.043 mag for V, $B-V$, and $V-I$, respectively.

As Table 6 shows, the differences between this work and the Jester et al. (2005) and Ivezić et al. (2007) versions of the transformed KIC photometry range from virtually zero to more than 0.04 mag. However, they also differ substantially from each other. The differences among the three calibration sources result entirely from differences in the transformation relations themselves, since the input KIC data are the same. So while there is a some uncertainty in the transformations between the KIC *griz* photometry and the *BVI* system, there are no indications of large systematic errors in the present photometry.

We conclude from this analysis that there are no systematic errors larger than about 0.02 mag between our photometry and the *UBVRI* system, as defined by the Landolt (2009) standard stars.

3. CLUSTER PROPERTIES—PHOTOMETRIC ANALYSIS OF NGC 6811

The combined full-field B, V and V, I photometry of NGC 6811 is shown in Figure 3; the different limiting magnitudes and field sizes of the several data sets are apparent in the diagram.

The figure illustrates that NGC 6811 is a relatively sparse cluster located in a moderately rich Milky Way field. Furthermore, the field of view covered by the three detectors we used in this program, which ranges from 13.3 arcmin on the Perkins Telescope to 42.8 arcmin (in a 2 × 2 mosaic) with the 2010 Hall Telescope data, is much larger than the visible cluster.

In fact, a large majority of the stars in this diagram belong to the field rather than the cluster. Nevertheless, a cluster main sequence is visible in the diagram, and there is a group of bright, red stars that could represent the red giant clump (that is, the population I analog of the horizontal branch—the core helium-burning stage of stellar evolution) of the cluster.

Table 6
Summary of This Work Minus the Transformed KIC Photometry

Calibration Source	ΔV	$\Delta(B-V)$	$\Delta(V-R)$	$\Delta(V-I)$
Jester et al. (2005)	-0.018 ± 0.003	-0.042 ± 0.002	...	0.045 ± 0.002
Ivezić et al. (2007)	-0.035 ± 0.003	0.008 ± 0.002	0.002 ± 0.004	0.015 ± 0.002
Equation (4)	0.032 ± 0.003	-0.017 ± 0.002	...	0.031 ± 0.002

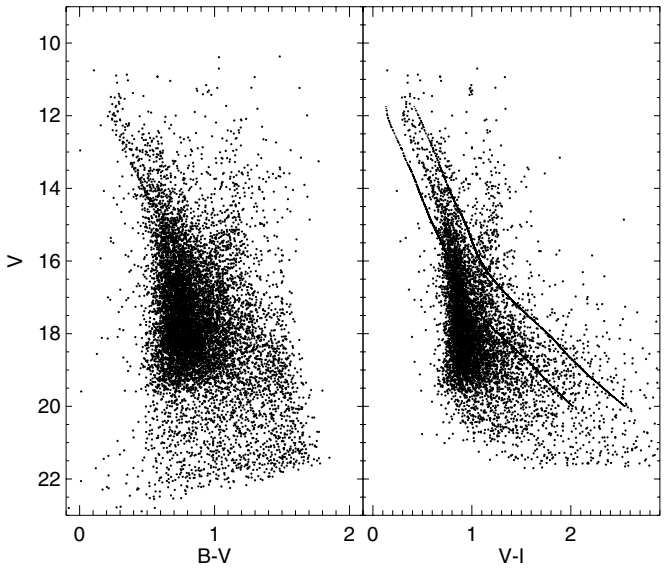

Figure 3. $[V, (B-V)]$ and $[V, (V-I)]$ color–magnitude diagrams for all stars in the catalog (Table 3). The effects of different field sizes and limiting magnitudes on different nights (see Table 1) are evident in the $B-V$ color–magnitude diagram. The solid lines in the $[V, (V-I)]$ CMD delineate the blue and red limits of the region we used to calculate the radial density distribution.

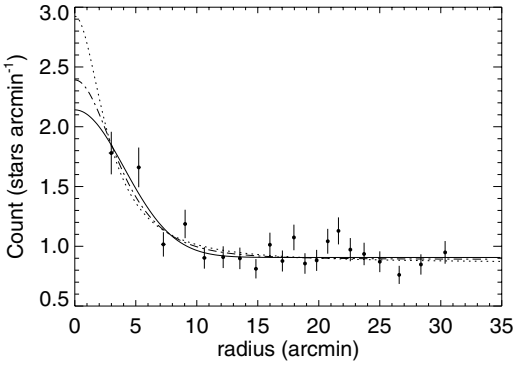

Figure 4. Radial star density profile for stars in the region of the CMD outlined in Figure 3. The errors in the radius values are of the order of 0.1 arcmin and are not shown. The solid, dotted, and dash-dotted lines represent the exponential, King, and Plummer model profiles (see Table 7), respectively.

3.1. Cluster Size and Richness

To estimate the cluster size and population, we counted stars in annular rings, assuming a central position for the cluster at R.A. $= 19^{\rm h}37^{\rm m}17^{\rm s}$, decl. $= 46^{\circ}23'18''$ (2000). As Figure 3 shows, the limiting magnitude of the photometry is not uniform over the cluster area, so to derive the cluster structural properties, we used only the V and I images from the night of 2005 September 30. On this night we obtained deep images in V and I over a 2×2 mosaic of $20'$ fields, with the southwest field centered on the cluster.

Rather than counting stars within fixed rings about the center, we elected to calculate the radii within which a fixed number of stars are located. In this way, we were able to derive star counts with moderately uniform statistical errors in each ring.

Therefore, beginning at the cluster center, we found the radius within which 100 stars are located. Then we counted from that radius to the next radius within which another 100 stars are located, and so on. The stellar density in each ring is 100 divided by the area between the inner and outer radii of the ring. Assuming that the stellar density is constant within each ring, the effective radius of the ring is the radius that divides the area of the ring into two equal sections.

With this procedure, the uncertainty of the count is zero—the count is always exactly 100 stars. Similarly the inner radius of a ring, defined as the outer radius of the previous ring, is fixed in advance of the count. So the Poisson statistical uncertainty translates into an uncertainty in the outer radius, making the area of the ring uncertain, in this case by 10%, i.e., by the square root of 100. Therefore, the errors in the stellar density and in the effective radius of the ring are defined by the 10% uncertainty in the area of the ring. Beyond a radius of 10 arcmin, the field of view does not cover a complete ring, so for the outer rings, we did a numerical integration of each incomplete ring to add correction factors to the areas.

To limit the contamination by the rich background of field stars, we restricted the counts to stars between magnitudes 11 and 18, within the solid lines shown in Figure 3. The blue and red edges of the region outlined in the figure are defined by a 1 Gyr, $Z = 0.009$, Yale–Yonsei (YY; Demarque et al. 2004) isochrone. To define the blue edge, we shifted the isochrone by 10 mag in V and -0.05 mag in $V-I$, and for the red edge, we shifted the isochrone by 9.25 mag in V and 0.15 mag in $V-I$.

The results of the radial star counts are shown in Figure 4. We used these counts to determine the cluster structural properties. We tried fits to three model radial cluster density profiles—a simplified King (1962) profile, assuming in effect an infinite tidal radius (see his Equation (13)):

$$\rho(r) = \rho_{cl}\left(1 + \frac{r^2}{r_c^2}\right)^{-1} + \rho_f, \tag{5}$$

a Plummer (1911) profile:

$$\rho(r) = \rho_{cl}\left(1 + \frac{r^2}{r_p^2}\right)^{-2} + \rho_f \tag{6}$$

(derived from Plummer's Equation (13)), and a simple exponential function:

$$\rho(r) = \rho_{cl}\,\exp\left(-r^2/\sigma_r^2\right) + \rho_f. \tag{7}$$

In these equations, ρ_{cl} refers to the peak of the radial stellar density distribution and ρ_f is the background field stellar density. The cluster core angular radius is defined by r_c, r_p, and σ_r, respectively, in the three equations.

Table 7
Fits to the Cluster Radial Star Density Profile

	Exponential	Plummer	King
Stars between magnitude 11 and 18			
Peak density	1.282 ± 0.252	1.447 ± 0.338	1.640 ± 0.482
Effective radius	6.742 ± 0.935	7.686 ± 1.573	4.404 ± 1.388
Background	1.111 ± 0.034	1.087 ± 0.039	1.041 ± 0.048
Stars between magnitude 11 and 15			
Peak density	0.766 ± 0.190	1.041 ± 0.345	1.734 ± 1.412
Effective radius	5.871 ± 0.865	5.825 ± 1.320	2.415 ± 1.409
Background	0.233 ± 0.016	0.214 ± 0.018	0.196 ± 0.021
Stars between magnitude 15 and 18			
Peak density	0.518 ± 0.178	0.575 ± 0.242	0.658 ± 0.334
Effective radius	7.766 ± 2.146	9.183 ± 3.692	5.355 ± 3.439
Background	0.901 ± 0.033	0.887 ± 0.039	0.864 ± 0.050

The parameters of the fits to the trial functions are given in Table 7 and the functions are plotted in Figure 4. Both the central density and the core radius have substantial uncertainties, as expected, given that it is a somewhat sparse cluster projected against a moderately rich stellar background. There are indications in the fits that the fainter stars are more widely spread out than the brighter, more massive, stars. Overall, the simple exponential is the best match to the cluster distribution; we will use that in the following analysis.

To estimate the number of cluster stars brighter than magnitude $V = 18$, we simply integrated the exponential density function of Equation (7) over all space after subtracting the background level:

$$N_{cl} = \pi \rho_{cl} \sigma_r^2. \quad (8)$$

We find about 183 cluster stars brighter than magnitude $V = 18$, but this is likely to be a substantial underestimate of the total cluster population. There are numerous reports in the literature (see, e.g., Perryman et al. 1998) of extended halos of cluster stars surrounding the visible cluster core region. If indeed there is such a halo of NGC 6811 stars, it is unlikely to be detectable photometrically against the dense background field. In any case, our goal is to obtain a well-defined cluster CMD, not necessarily a complete sample of all cluster stars.

The CMD of the central 6 arcmin radius region of the cluster is shown in Figure 5. The main sequence is more clearly distinguished than it is in Figure 3, and several stars remain at the expected location of the red giant clump.

The upper diagram of Figure 6 shows counts in one magnitude bins of stars located within the blue and red limits shown in Figure 3. The open squares are derived from stars beyond 20 arcmin from the cluster center and the filled circles are the equivalent counts of stars in the central 10 arcmin region of the cluster. The counts for stars in the outer region have been corrected for the differences in the areas of the two regions. The lower diagram of the figure shows the differences between the counts, where the error bars refer to the Poisson errors of the counts.

Between magnitudes 11 and 18, the star counts are consistent with a more or less flat cluster luminosity function, of the order of 20 stars per magnitude interval. There is little evidence for a significant population of cluster stars fainter than magnitude 18, although the combination of the dense field star population and a possible increase in the cluster radius could mask a considerable number of cluster stars. Even in the central region of the cluster, as can be seen in Figure 5, most of the stars are non-members. We have undertaken a separate study to identify radial velocity members of a wider area around the cluster. Although this study is still incomplete (S. Meibom et al., in preparation; see also Meibom et al. 2011a), we have identified over 200 candidate cluster members. We will use these radial velocity members as our actual sample for the Markov Chain Monte Carlo (MCMC) analysis in Section 4.

3.2. Estimates of the Cluster Reddening and Composition

The version of the galactic infrared dust emission map of Schlegel et al. (1998) archived at http://irsa.ipac.caltech.edu/applications/DUST/ predicts a total reddening along the line of sight toward NGC 6811 of $E(B - V) = 0.154 \pm 0.002$. Since the Schlegel map shows the total galactic dust along each line of sight, this value represents a maximum estimate of the reddening to the cluster. NGC 6811 has a galactic latitude about 12°, with a distance of just under 1 kpc, as we show in the following, so the cluster is about 200 pc from the galactic plane. At that location, most, but not necessarily all, of the dust should ordinarily be expected to be in front of the cluster.

Another reddening estimate and the metallicity can be derived from the colors of the red giant clump stars. In Figure 3, there are several likely red giant clump stars located near $V = 11.30$ and $B - V = 0.95$. Radial velocities of five stars selected from Meibom et al. (2011a) confirm that they are likely cluster members. Since the position of the red giant clump is a strong function of metallicity, but a weak function of cluster age, it can be used to put some constraints on the reddening and metallicity. Table 8 shows the available photometry for the five cluster giants; the star numbers are taken from Table 3, except for the star KIC9532903, for which we do not have photometry.

A final reddening estimate can be derived using the Padova stellar models (Girardi et al. 2010) which include the helium-burning main-sequence phase of evolution (i.e., the red giant clump). We created synthetic CMDs of the red giant region using 1 Gyr Padova isochrones (close to the age we derive for the cluster) with three different metallicities ($Z = 0.006$, 0.012, and 0.018), by picking 250 stars at random masses from the models. In this way, we created CMDs with realistic distributions of stars by luminosity and color. Figure 7 shows CMDs for the three isochrones, shifted to an arbitrary distance modulus of 9.5 mag for clarity. The individual giant stars from Table 8 are plotted in the figure as filled symbols.

Since the actual NGC 6811 giant stars in Figure 7 are reddened whereas no reddening was added to the synthetic CMDs, the difference between the color of the NGC 6811 stars and the mean color of any of the synthetic CMDs represents

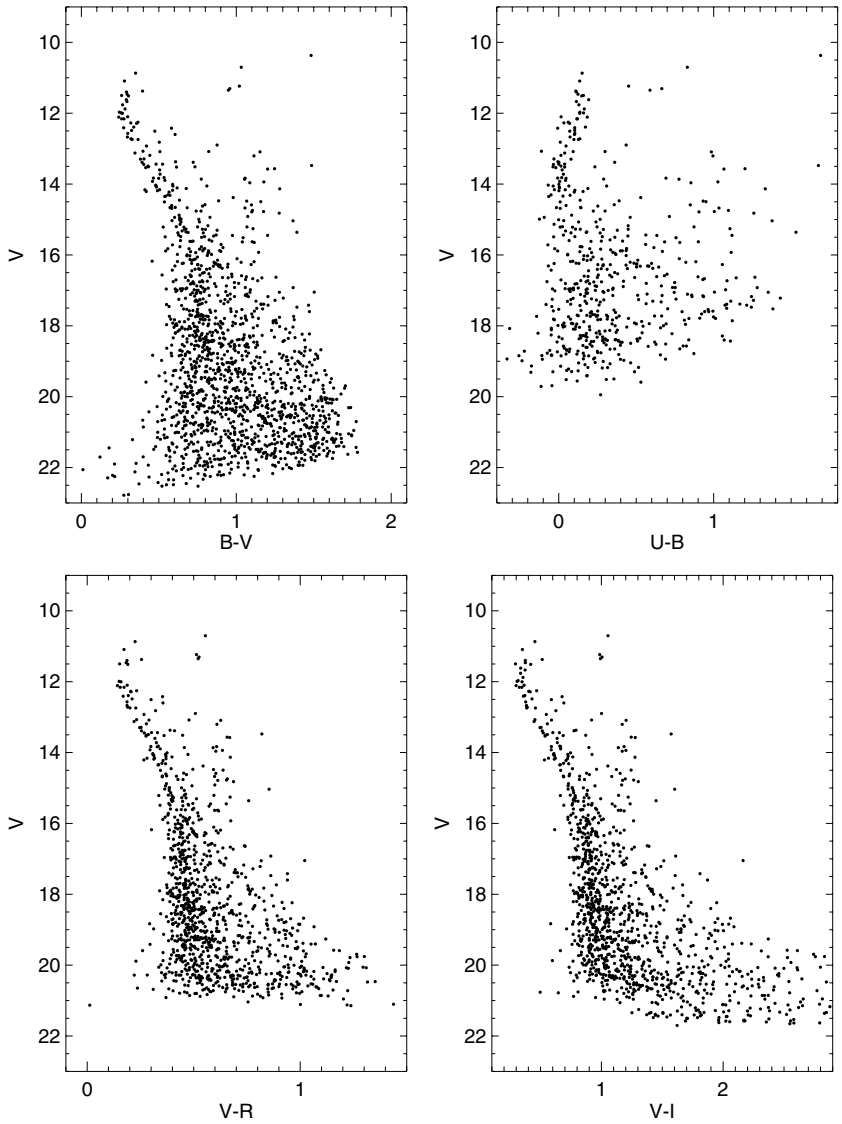

Figure 5. $[V, (B-V)]$, $[V, (U-B)]$, $[V, (V-R)]$, and $[V, (V-I)]$ color–magnitude diagrams for stars within a 6 arcmin radius of the cluster center. Within this radius, the photometry has a nearly uniform limiting magnitude across the entire field.

the amount of reddening the cluster would have if it had the corresponding metallicity. Thus, assuming that the stars in Table 8 actually are red giant members of the cluster and that the cluster is relatively close to 1 Gyr in age, a solar metallicity would imply essentially zero reddening; conversely, for a reddening as high as 0.15, the cluster would have to be very metal-poor. Either of those possibilities would be surprising, given the galactic environment of the cluster. So, unless there is a serious problem with either the photometry or the models, the reddening to the cluster is relatively small, and its metallicity is less than solar.

4. FITTING THEORETICAL MODELS TO THE NGC 6811 CMD—A BAYESIAN ANALYSIS

It is well known that there are degeneracies in the observed color indices of stars with different physical properties (temperature, composition, and reddening). That is, one star may appear redder than another because it is cooler or because of interstellar reddening or higher metallicity. At the same time, it appears deceptively easy to extract the physical properties of stars in a cluster from the appearance of the cluster CMD. A common practice is to "fit" isochrones to cluster CMDs simply by shifting the isochrone sequences until there is a good visual match. However, such a solution is generally not unique, and there is no quantitative measure of the uncertainty of the results. In many cases, isochrones with a wide range of ages and compositions can be made to appear to fit the same cluster sequence.

If there is independent information about a cluster, so that reddening or metallicity, for example, has been determined by other methods (or perhaps simply assumed by some argument), then some of the photometric degeneracy is removed. Nevertheless, for many clusters it is necessary to rely on photometric criteria alone to define the cluster parameters. To some degree, multiple color indices can help to remove the degeneracies, particularly when a color index such as $U-B$ is available. But that still leaves the problem of defining a quantitative determination of the cluster properties and their uncertainties.

4.1. Bayesian Analysis—The MCMC Algorithm

A variety of quantitative analytic approaches have been taken to derive cluster properties, with varying degrees of success (see Monteiro et al. 2010 or Janes & Hoq 2011 for recent discussions

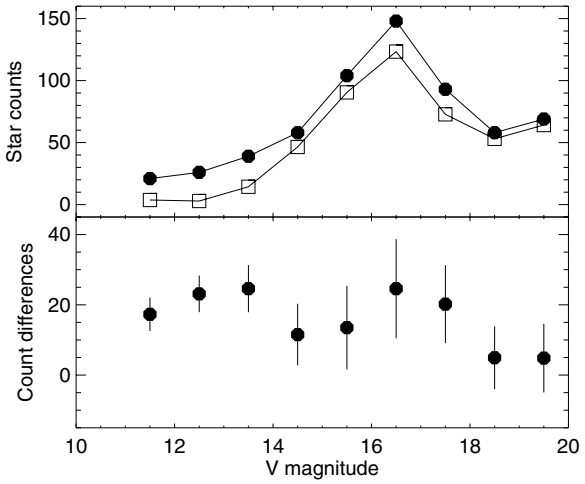

Figure 6. Upper diagram: star counts for stars in the field region around the cluster, beyond 20 arcmin from the cluster center (open squares) and for stars within 10 arcmin of the cluster center (filled circles). The field region counts have been corrected for the differences in the areas of the two regions. The star counts include only stars within the limits shown in Figure 3. Lower diagram: differences in the counts between the cluster stars and the field stars. The error bars represent Poisson statistics in the counts.

of the problem). In a series of papers, von Hippel et al. (2006) (see also De Gennaro et al. 2009 and references therein) have applied Bayesian statistical methods to derive cluster properties. For a general reference to Bayesian methods, see Press et al. (2007) and for some additional astronomical applications of Bayesian analysis, see Ford (2005), Gregory (2005), or Burke et al. (2007). Bayes' theorem states that

$$P(\mathbf{m}|\mathbf{D}) = \frac{P(\mathbf{m})\mathcal{L}(\mathbf{D}|\mathbf{m})}{P(\mathbf{D})}, \quad (9)$$

where **D** represents the data set and **m** is the set of model parameters. The goal is to find the posterior probability distribution function (PDF), $P(\mathbf{m}|\mathbf{D})$, given a prior PDF, $P(\mathbf{m})$, of model parameters and a likelihood distribution, $\mathcal{L}(\mathbf{D}|\mathbf{m})$. The probability of the data, $P(\mathbf{D})$, is essentially the integral of the numerator of Equation (9) over all possible model parameters, **m**, and is ordinarily difficult to compute. However, it is effectively a normalizing constant, and so the important properties of the posterior distribution, such as means and standard deviations, can be found from Equation (9) without knowing $P(\mathbf{D})$.

The MCMC algorithm provides an efficient mechanism for sampling the posterior distribution without the necessity of calculating the denominator of Equation (9). Our approach is similar in many respects to that of von Hippel et al. (2006) who described a Bayesian approach to fitting stellar models to a star cluster CMD including white dwarf stars. Our procedure is different in some details, partly because the NGC 6811 white dwarf stars are much too faint and the cluster is nearly obscured by field stars. Our data consist of V magnitudes plus $(B-V)$, $(U-B)$, $(V-R)$, and $(V-I)$ color indices of stars assumed to be on the main sequence.

The MCMC method begins with the selection of a distribution of priors, $P(\mathbf{m})$, which constitute an assumed model of the problem. Our model includes the distance modulus, reddening, age, metallicity, and a selected set of isochrones. For the range of the parameters, we chose 0.03–0.12 mag for the reddening, 9.75–10.50 mag (YY) and 10.0–10.75 mag (Padova) for the distance modulus, 0.70–1.40 Gyr for the age and 0.005–0.017 for Z, the metallicity.

Table 8
Photometry of Red Giant Clump Stars

Star	Index	(1)	(2)	(3)	Mean
101	V	11.157	11.159	10.981	11.099
	$B-V$	0.938	0.952	0.909	0.933
	$U-B$	0.630	0.619	···	0.624
	$V-R$	···	···	···	···
	$V-I$	0.995	···	0.956	0.976
118	V	10.703	10.675	10.648	10.675
	$B-V$	1.032	1.030	0.984	1.015
	$U-B$	0.830	0.800	···	0.815
	$V-R$	0.555	···	···	0.555
	$V-I$	1.054	···	1.047	1.050
3202	V	11.350	11.372	11.334	11.352
	$B-V$	0.949	0.936	0.957	0.947
	$U-B$	0.589	0.619	···	0.604
	$V-R$	0.521	···	···	0.521
	$V-I$	0.992	···	0.937	0.964
3278	V	11.235	11.236	11.186	11.219
	$B-V$	1.020	0.944	0.952	0.972
	$U-B$	0.451	0.589	···	0.520
	$V-R$	0.513	···	···	0.513
	$V-I$	0.986	···	0.947	0.966
KIC9532903	V	···	11.172	11.152	11.162
	$B-V$	···	0.954	0.948	0.951
	$U-B$	···	0.642	···	0.642
	$V-R$	···	···	···	···
	$V-I$	···	···	0.979	0.979

Notes. (1) Table 3. (2) Glushkova et al. (1999). (3) KIC (Brown et al. 2011) using Equation (4).

At each iteration, after choosing an isochrone of a particular age and metallicity, shifted by some distance modulus and reddening (these are the priors), we calculated a likelihood function that the photometry could be drawn from the isochrone. As shown in Equation (9), the posterior PDF is proportional to the product of the prior PDF, $P(\mathbf{m})$ and the likelihood function, $\mathcal{L}(\mathbf{D}|\mathbf{m})$. For the priors (age, Z, reddening, and distance modulus), we assumed a uniform probability over the linear space of the parameters as specified in the previous paragraph, so they simply consist of constants in the prior distribution.

For the likelihood distribution itself, we computed a sequence of 1000 theoretical stars at each iteration drawn with random masses from the selected isochrone to create a theoretical CMD. We considered this CMD to be error free, in the sense that the colors and magnitudes of the theoretical stars were taken from a direct interpolation in the isochrone. The likelihood function is defined by a comparison of the observed photometry with this theoretical CMD. By choosing a discrete CMD of theoretical stars we removed one of the common problems in fitting isochrones to data. Typically, an isochrone is drawn as a line passing through all the evolutionary stages represented at a particular age. But in fact, for considerable parts of that path, particularly along parts of the subgiant and giant branches, there is a low probability that there will actually be any stars. Those stretches of the isochrone do not contribute significantly to the solution.

Therefore, given a photometric index, k, for a target observed star, i, we calculated the distances (in photometric space) between the star and each of the theoretical stars, j. The quantity,

$$z_{ij} = \left[\frac{\sum_k (O_{ik} - T_{jk})^2}{\sum_k \sigma_{ik}^2}\right]^{1/2}, \quad (10)$$

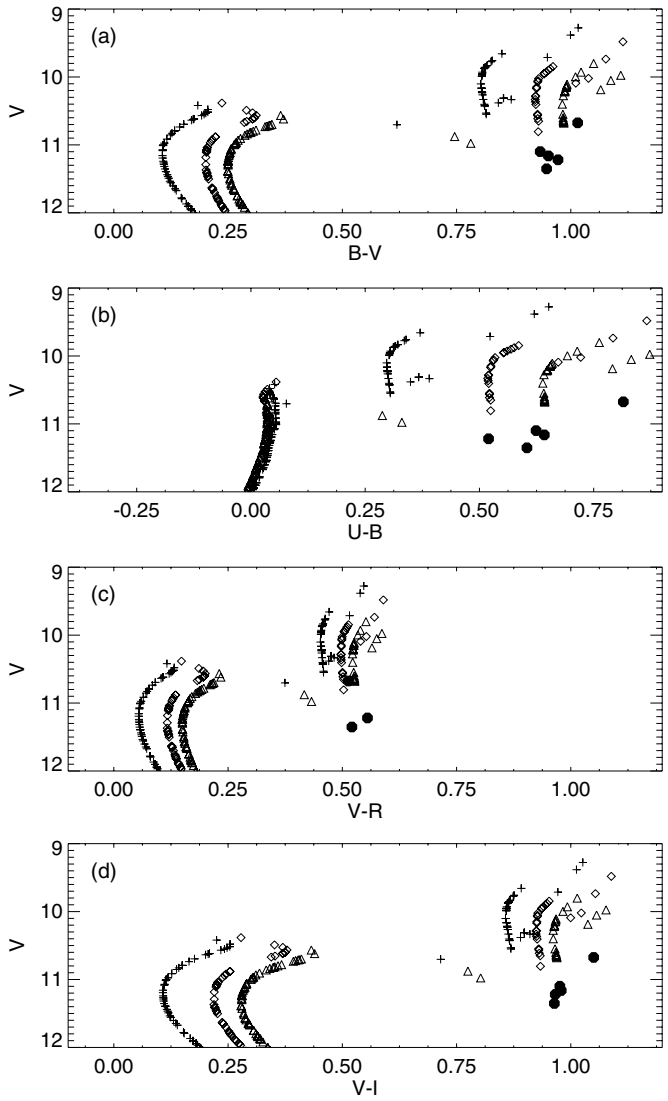

Figure 7. Model CMDs for the main-sequence turnoff and giant branch regions for three different 1 Gyr Padova isochrones. The red giant clump stars from Table 8 are shown as filled symbols. Plus signs indicate $Z = 0.006$ models, diamonds are $Z = 0.012$ models, and triangles are $Z = 0.018$ (solar) models. (a) $V, B - V$; (b) $V, U - B$; (c) $V, V - R$; (d) $V, V - I$. The model stars are shifted in V by an arbitrary 9.5 mag for clarity, so the vertical displacements between the model stars and the observed ones should be ignored. We conclude from this figure that the reddening must be less than 0.015 mag and/or that the metallicity must be less than solar.

is a measure of the rms differences between the observed photometric indices, O_{ik} (i.e., V magnitude and one or more color indices), of star i and the corresponding theoretical indices, T_{jk}, of star j in units of the photometric errors, σ_{ik}. The probability that z_{ij} could be as small as it is by chance is given by $\mathrm{erf}(z_{ij})$, the error function of z_{ij}. So now, the probability that the observed star could be drawn from the CMD of theoretical stars is one minus the product of the inverse probabilities of the z_{ij} values of all the theoretical stars, i.e.,

$$p_i = 1.0 - \prod_j [\mathrm{erf}(z_{ij})]. \tag{11}$$

There will typically be some range of theoretical stars that could match the target star with finite probability, but in practice, only a few of the theoretical stars lie close to the target observed star in the CMD. The probability that the observed star could be drawn from the rest of the theoretical stars is effectively zero (that is, $\mathrm{erf}(z_{ij}) \simeq 1$) so they do not contribute to the product in Equation (11). Assuming a Gaussian distribution of differences between the target observed star and each of the nearby theoretical stars, p_i represents the cumulative probability that the observed star could be drawn from the theoretical CMD.

Now the likelihood function becomes

$$\mathcal{L}(\mathbf{D}|\mathbf{m}) = \prod_i \{p_i\}. \tag{12}$$

To make the problem computationally manageable, we actually calculate the function

$$\mathcal{L}_l(\mathbf{D}|\mathbf{m}) = \sum_i ln\ p_i. \tag{13}$$

So now, the full (logarithmic) Bayesian model is just

$$P_l(\mathbf{m}|\mathbf{D}) = P(\mathbf{m})\mathcal{L}_l(\mathbf{D}|\mathbf{m}). \tag{14}$$

In principal, the distribution given by Equation (14) could be developed by randomly trying all possible combinations of the parameters, but the MCMC method using the Hastings-Metropolis algorithm (see von Hippel et al. 2006; Ford 2005; Gregory 2005) provides an efficient mechanism for sampling the distribution. The key to the algorithm is to develop a jump probability function or candidate transition probability distribution $q(\mathbf{m}_t|\mathbf{m})$ to determine the transition from model m to a trial model m_t in such a way that the subsequent set of parameters depends on the current set, but not on any previous values. The complete requirements for the jump functions are discussed in the references cited above; for the present problem a transition from the present value of any of the parameters to a new trial value can be determined by selecting a random number with a Gaussian distribution centered on the current value. The scaling factor for the size of the jumps is set by experiment, as described below.

Once a new candidate set of parameters has been chosen according to the jump functions, Equation (14) can be evaluated with the new parameters, and the result can be compared with the previous value. The new trial is accepted or not according to a transition probability distribution, $\alpha(\mathbf{m}_t|\mathbf{m})$, where $\mathbf{m}_t$ refers to the trial model. If the jump sizes are too small, the chain will take too long to traverse the parameter space; if they are too large, too many of the trials will be rejected. The jumps are often adjusted in the initial stages of an MCMC run, known as a burn-in period. For the present problem, with a simple model and only a few parameters, we simply ran an extensive series of trial runs with different jumps, until we achieved a satisfactory sampling efficiency.

The transition probability distribution is given by

$$\alpha(\mathbf{m}_t|\mathbf{m}) = min\left\{\frac{P(\mathbf{m}_t|\mathbf{D})}{P(\mathbf{m}|\mathbf{D})}\frac{q(\mathbf{m}|\mathbf{m}_t)}{q(\mathbf{m}_t|\mathbf{m})}, 1\right\}. \tag{15}$$

When the proposal distributions are symmetrical, as in this case, $q(\mathbf{m}|\mathbf{m}_t) = q(\mathbf{m}_t|\mathbf{m})$. A trial solution is accepted as the next iteration if α exceeds a random number chosen on the range 0–1. This approach ensures that improved solutions are always selected, but it also allows the procedure to search the entire parameter space.

There are several other complications in the present problem. First, there are tight correlations among the variables—for

Table 9
Summary of MCMC Chains

	$E(B-V)$	$(m-M)$	Age (Gyr)	Metallicity (Z)
Radial velocity members ($U-B$, $B-V$, $V-R$, $V-I$)				
YY models chain 1	0.068 ± 0.010	10.126 ± 0.078	1.097 ± 0.066	0.012 ± 0.001
Chain 2	0.068 ± 0.010	10.126 ± 0.078	1.096 ± 0.067	0.012 ± 0.001
Chain 3	0.068 ± 0.010	10.126 ± 0.080	1.096 ± 0.068	0.012 ± 0.002
Padova models chain 1	0.083 ± 0.010	10.327 ± 0.086	0.930 ± 0.057	0.012 ± 0.002
Chain 2	0.083 ± 0.010	10.327 ± 0.085	0.930 ± 0.057	0.012 ± 0.002
Radial velocity members ($B-V$ only)				
YY models	-0.001 ± 0.052	10.087 ± 0.245	1.044 ± 0.182	0.019 ± 0.010
Padova models	0.165 ± 0.062	10.447 ± 0.258	0.973 ± 0.182	0.005 ± 0.004
Radial velocity members – floating zero points ($U-B$, $B-V$, $V-R$, $V-I$)				
YY models	0.066 ± 0.025	10.127 ± 0.187	1.059 ± 0.189	0.012 ± 0.004
Padova models	0.081 ± 0.015	10.306 ± 0.111	0.942 ± 0.076	0.012 ± 0.002
Synthetic Padova CMDs ($E(B-V) = 0.075$; $(m-M) = 10.0$; Age $= 1.0$; $Z = 0.012$)				
YY models	0.077 ± 0.038	9.899 ± 0.145	1.183 ± 0.121	0.010 ± 0.002
Padova models	0.075 ± 0.031	10.002 ± 0.138	0.987 ± 0.104	0.012 ± 0.003
Synthetic Yale CMDs ($E(B-V) = 0.075$; $(m-M) = 10.0$; Age $= 1.0$; $Z = 0.012$)				
YY models	0.071 ± 0.027	9.995 ± 0.206	0.984 ± 0.147	0.012 ± 0.004
Padova models	0.077 ± 0.027	10.241 ± 0.175	0.767 ± 0.079	0.018 ± 0.005

instance, the effects of a cluster's reddening and its metallicity are similar. Furthermore, the isochrones are available only at discrete intervals of the age and metallicity. Finally, many of the stars in the cluster region are non-members and others are binary stars. Even the radial velocity sample we used for the MCMC analysis is somewhat contaminated with binaries and non-members that happen to have similar velocities to the cluster. These problems together mean that the transition probability distribution can lead to the rejection of almost all trial solutions, or the chain can become stuck in secondary probability peaks.

Gregory (2005) described the addition of a "tempering" parameter analogous to the temperature parameter used in simulated annealing algorithms—see, e.g., Ford (2005). So now we can replace Equation (14) with

$$\pi(\mathbf{m}|\mathbf{D}) = P(\mathbf{m}) \exp[\beta P_l(\mathbf{D}|\mathbf{m})], \quad (16)$$

where $1 > \beta > 0$ is the tempering parameter. When $\beta = 1$, then $\pi(\mathbf{m}|\mathbf{D}) = P(\mathbf{m}|\mathbf{D})$, the desired distribution. To avoid the problem of too many trial rejections, we adopted the following procedure for running the Markov chain: We first set $\beta = 1$, and if the first trial proposal was accepted, we saved the results of that trial. But if the proposal was not accepted, we set β equal to the inverse of the square of the number of successive failures, thereby increasing the "temperature" of the distribution at each pass through the loop. When a trial was finally successful, we reset β to one, but we did not save that trial. In this way we saved only successful trials when $\beta = 1$, the desired value. This procedure also means that by saving only occasional trials, we removed any residual short-term correlations, as described by von Hippel et al. (2006).

Once the Markov chain has converged, the subsequent history of the chain consists of a sequence of random samples from the posterior PDF. The results can be displayed as histograms of marginal distributions of the various parameters for which the statistical properties can be evaluated.

Ford (2005) discusses the question of convergence of the chain to an equilibrium distribution. As a practical matter, convergence can be tested by comparing multiple independent Markov chains; if there is convergence, all the relevant statistical parameters will be the same within the statistical uncertainties. As discussed below, we ran several chains, including ones where we used different starting values for the parameters. For this problem, with only four parameters, convergence was very rapid—typically in a few hundred iterations, as we show in the following section.

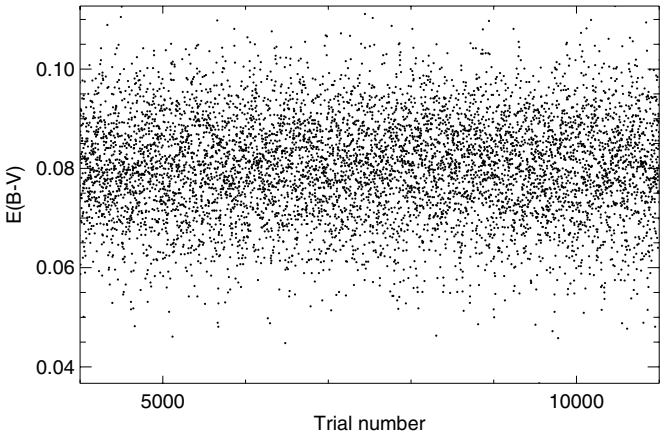

Figure 8. Sample of trial values of $E(B-V)$ from one MCMC chain. Trials from 4000 to 11,000 are shown. No evidence for correlations between successive trials and $E(B-V)$ are visible.

4.2. MCMC Results

The result of the MCMC analysis is the distribution of the numbers of successful trials as a function of the various parameters. The marginal distribution of each parameter, found by integrating over all values of the other parameters, is proportional to the posterior PDF of that parameter; the statistical properties (the mean, standard deviation, etc.) of the two distributions are the same.

As described above, S. Meibom et al. (in preparation) have identified a number of stars with radial velocities consistent with membership in the cluster (see also Meibom et al. 2011a). We used these stars as the data set for the MCMC analysis. In most of the MCMC trials, we used all four of the color indices ($B-V$, $U-B$, $V-R$, and $V-I$) in the catalog.

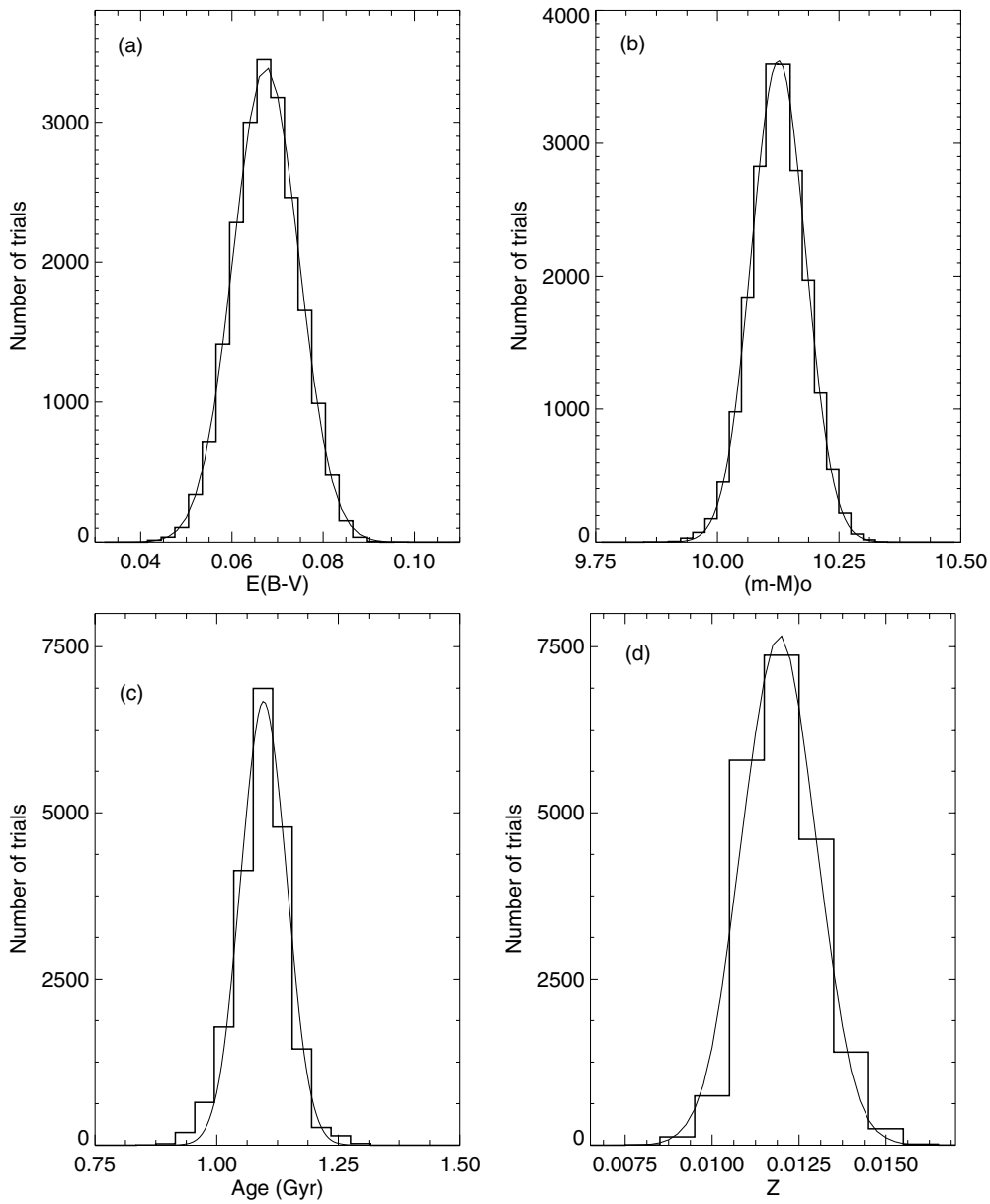

Figure 9. Marginal distributions of cluster properties for YY chain 1. Number of samples vs. (a) reddening, $E(B-V)$, (b) distance modulus, (c) age in Gyr, and (d) metallicity, Z. In each figure, the solid curve represents a Gaussian fit to the distribution (see Table 9).

Table 10
NGC 6811—Summary of MCMC Analysis

	$(m-M)$	$E(B-V)$	Age (Gyr)	Z	[Fe/H]
YY models	10.13 ± 0.19	0.066 ± 0.025	1.06 ± 0.19	0.012 ± 0.004	-0.18
Padova models	10.30 ± 0.11	0.081 ± 0.015	0.94 ± 0.08	0.012 ± 0.002	-0.20
Mean values	10.26 ± 0.18	0.074 ± 0.024	1.00 ± 0.17	0.012 ± 0.004	-0.19

For our age and metallicity model, we used two sets of isochrones—the YY isochrones (Demarque et al. 2004—see also www.astro.yale.edu/demarque/yyso.html) and the Padova set of isochrones (Girardi et al. 2010; Marigo et al. 2008—which can be found at stev.oapd.inaf.it/cgi-bin/cmd). Using interpolation software in the respective web sites, we computed grids of isochrones with ages ranging from 0.4 to 1.6 Gyr in age in 0.01 Gyr increments and with metallicity, Z, ranging from 0.001 to 0.030 in 0.001 increments, on a scale where the Sun has a value of 0.0182 (YY isochrones) or 0.019 (Padova isochrones). We shifted the isochrones in distance modulus and reddening; for our initial reconnaissance we sampled distance modulus values from 9.25 to 10.75 and reddening from $E(B-V) = 0.0$ to $E(B-V) = 0.15$ in increments of 0.01 mag. We later tightened the sampling range on all the parameters. We used color excess ratios based on Dean et al. (1978) and Bessell et al. (1998): $E(U-B)/E(B-V) = 0.89$, $E(V-R)/E(B-V) = 0.60$, and $E(V-I)/E(B-V) = 1.30$.

We ran several independent MCMC chains with randomly selected values of the input parameters. In each chain, we did

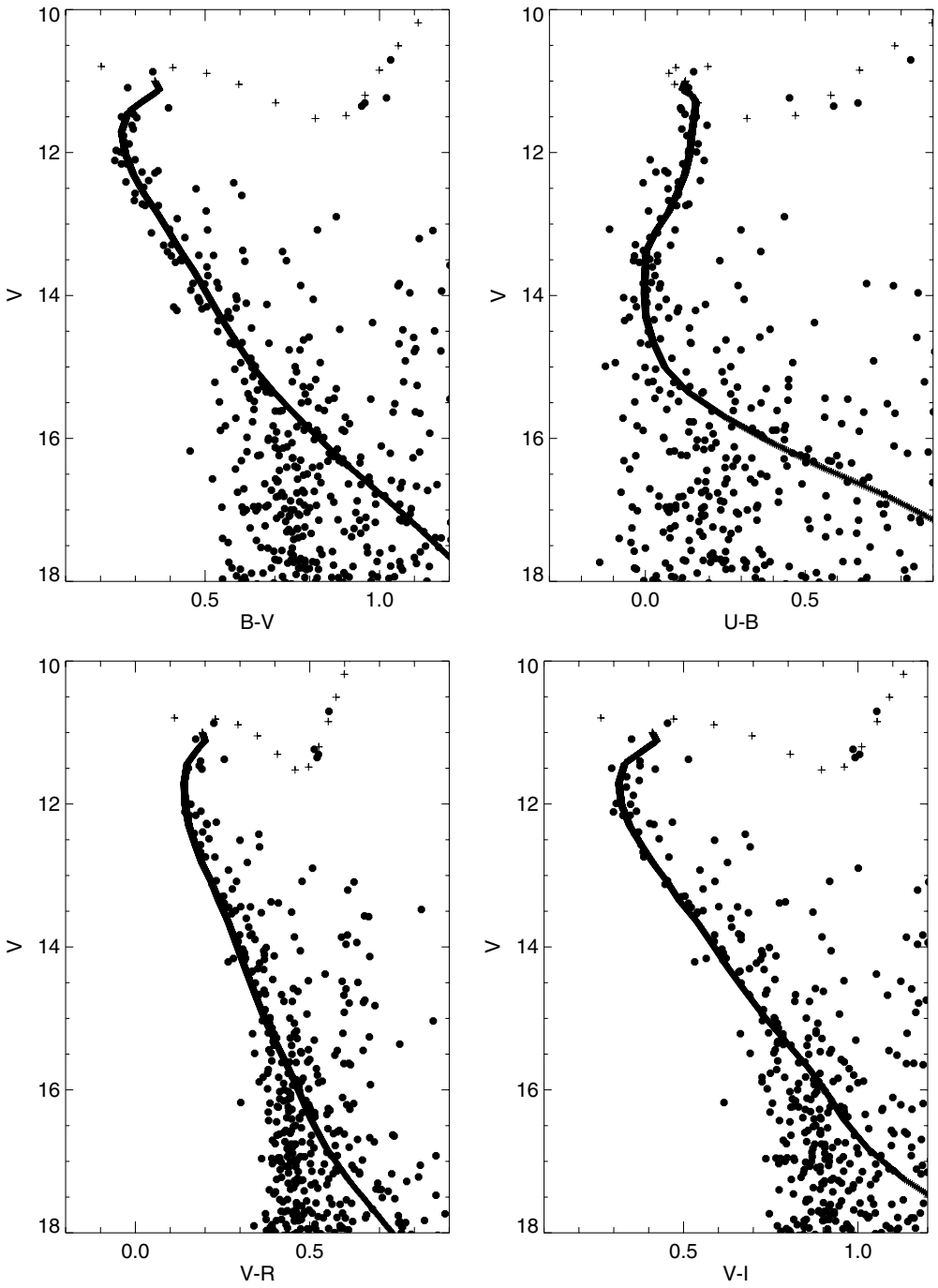

Figure 10. CMDs showing all stars within 6 arcmin of the cluster center, as in Figure 5. The plus signs, which appear as a solid line along the main sequence, represent a 1.06 Gyr, $Z = 0.012$ synthetic YY CMD, shifted to $(m - M) = 10.13$, $E(B - V) = 0.066$. (See Table 9.)

250,000 trials. With our procedure, typically about 20,000 or more trials were saved. Table 9 shows the results from the various MCMC chains. For three YY chains the results of the Gaussian fits to the marginal distributions were virtually identical. Similarly, the two Padova chains were essentially identical to each other. That does not mean that the cluster parameters are accurate to that precision, but only that the PDFs have converged, and are repeatable at that level, even though the starting values were different for each chain.

To illustrate that the values in successive trials are random samples from the probability distribution of clusters properties, Figure 8 shows a short sequence of successful trial reddening values from YY chain 1. There are no indications of correlations from one saved trial to the next.

Figure 9 shows the marginal distributions for our first chain with the YY isochrones. We fitted Gaussian functions to the marginal distributions and took the peaks of these Gaussians as the maximum-likelihood estimator of the parameters and the Gaussian sigmas as estimators of the uncertainties.

We also tried MCMC chains using just V and $(B - V)$. The YY and Padova runs yielded reddening and metallicity values rather different both from each other and from the chains where we

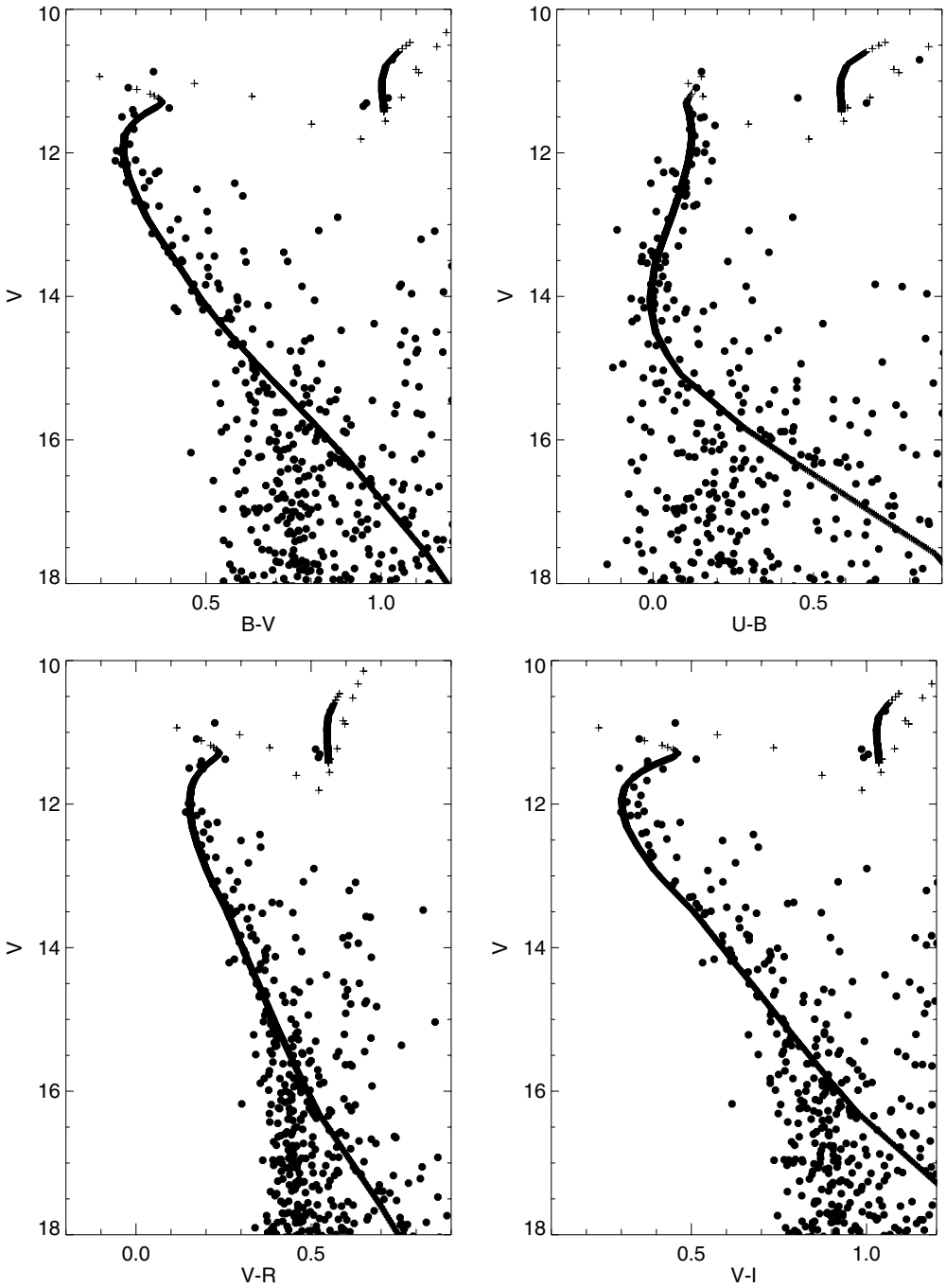

Figure 11. Same as Figure 10 except overlaid with a 0.942 Gyr, $Z = 0.012$ synthetic Padova CMD, shifted to $(m - M) = 10.306$, $E(B - V) = 0.081$. (See Table 9.)

included all indices. Perhaps more significantly, the calculated uncertainties are very much larger than in the previous cases. This is the expected result—with a single color index, it is not usually possible to "fit" stellar isochrones to observed CMDs unambiguously. In the language of the Bayesian analysis, the PDFs in the two cases are broad and not well defined.

For these initial solutions, we assumed no uncertainty in the models and no zero-point errors in the photometry. Any model uncertainties are beyond the scope of this paper (but see Section 5); however, the MCMC procedure permits us to add priors for possible zero-point shifts. At each trial solution in the MCMC chain, we added a randomly chosen zero-point shift to each color index with a Gaussian distribution, centered on zero, and a sigma of 0.01 mag. We ran one chain each for the YY and Padova isochrones; the results are shown in Table 9. As expected, the widths of the PDFs are substantially larger, but the mean values have changed little. We consider these values to be the appropriate solutions and errors in the context of the two sets of models.

Figures 10 and 11 show CMDs of all stars within 6 arcmin of the cluster center (the same stars as in Figure 5). The plus signs (which run together along the main sequence) represent the locus of a sequence of 1000 stars chosen at equal mass intervals, derived from the isochrones based on the parameters from Table 9 for the chains with a floating zero point. The synthetic CMD in Figure 10 was created from a YY isochrone, with $E(B - V) = 0.066$, $(m - M) = 10.127$, age $= 1.06$ Gyr, and $Z = 0.012$, and the one in Figure 11 is based on a Padova

isochrone with $E(B-V) = 0.081$, $(m-M) = 10.306$, age = 0.94 Gyr, and $Z = 0.012$. The two sets of synthetic CMDs differ somewhat from one another and neither one is a perfect match to the shape of the observed cluster CMD.

4.3. Synthetic CMDs—Verification of the Bayesian Analysis

To verify our MCMC analysis, we created synthetic multicolor CMDs from both the Padova and YY isochrones. We selected 1 Gyr, $Z = 0.012$ isochrones and as in the previous section, we selected 1000 stars at equal mass intervals from the isochrones. We shifted the CMDs to a distance modulus of 10.0 and a reddening value of $E(B-V) = 0.075$. We added Gaussian noise to the simulated photometry with $\sigma = 0.015$, except for $(U-B)$ to which we added 0.030 noise. We then ran both sets of CMDs through the MCMC analysis using both sets of isochrones. The results of this test (see Table 9) show that when we analyzed the synthetic CMDs with the matching isochrones, the MCMC analysis reproduced the input parameters almost exactly. However, when we used the Padova isochrones to analyze the Yale synthetic CMD, and vice versa, there were definite offsets between the input CMD values and the calculated parameters.

As illustrated in Table 9, the same pattern persists through all of our MCMC chains; the Padova isochrones yield systematically larger reddening and distance modulus, but lower age than the YY isochrones even when we analyzed the same set of observed or synthetic photometry. These differences, amounting to approximately 0.2 mag in distance modulus, 0.1 Gyr in age and 0.015 mag in reddening, reflect real differences in the two sets of models near age 1.0 Gyr. The model differences are noticeable in Figures 10 and 11.

The variances we injected into the synthetic CMDs are slightly larger than the typical errors in the brighter observed stars, but the real stars include possible binaries and nonmembers. Furthermore, the widths of the marginal PDFs also depend to some degree on the distribution of stars along the CMD. So, for example, the star colors near the turnoff are much more sensitive to age than the colors of stars further down on the main sequence. The overall similarity of the PDFs for the fits to the observed and synthetic CMDs is indicative of the robust nature of the MCMC procedure.

5. DISCUSSION

The widths of the marginal distributions in Figure 9 represent the full range of the uncertainties in the cluster parameters, *within the context of the observed photometric indices, the stars selected for analysis and the theoretical models only*. However, the details of model color transformations and other model limitations will not seriously affect the shapes of these distributions, so the actual uncertainties in the Padova and YY models must be at least as large as the differences between them. The broader issue of model uncertainties and isochrone ages is beyond the scope of this paper—see, e.g., Gallart et al. (2005), Mamajek et al. (2009), or Soderblom (2010) for papers discussing models and the ages of stars.

So, for this paper, we consider the theoretical uncertainty to be simply the differences between the YY and Padova models. Our final values of the cluster properties, shown in Table 10, are the average of the YY and Padova solutions that include the possible systematic errors. For the uncertainties, we have added the model differences in quadrature with the calculated fitting errors, as shown in Table 9.

Our analysis illustrates the practical limitations in matching observed CMDs to theoretical isochrones. For example, when we limited our analysis to just the $(B-V)$ color index, we found a considerable difference in the maximum-likelihood color excess, $E(B-V)$ and the metallicity, Z, between the two sets of models. The YY chain settled on low reddening and high metallicity whereas for the Padova models the procedure found a maximum at higher reddening and very low metallicity. Because the effects of metallicity and reddening on the $B-V$ color index are almost the same, it is likely that small differences in the photometry or the distribution of cluster stars along the main sequence could make a large change in the solutions in this particular case.

In Section 3.2, we showed that there is some disagreement about the cluster reddening and metallicity. However, unless there are problems with model color transformations or large systematic errors in our photometry, the MCMC analysis gives values about midway between the two extremes we found in Section 3.2. We note specifically that, as shown in Figure 7, the colors of the red giant clump stars (all of which are well observed—see Table 8) are rather blue, which requires low metallicity and/or low reddening. An independent determination of either the reddening or the metallicity would be required to put additional constraints on either the Bayesian solution or a more traditional isochrone fitting analysis.

We thank the referee, Ted von Hippel, for his thorough and helpful review of this paper, and we want to acknowledge the financial and technical support from Boston University and Lowell Observatory. S.A.B. is grateful for financial support from the Barnes and LoMonaco families, and thanks the Flagstaff Public Library for providing a serene working environment during a crucial phase of this work. K.A.J. thanks Chris Burke for pointing out the power of Bayesian statistics. S.M. acknowledges support from NASA cooperative agreement NNX09AH18A (the *Kepler* Cluster Study).

Facilities: Perkins (PRISM)

REFERENCES

Barkhatova, K. A., Zakharova, P. E., & Shashkina, L. P. 1978, SvA, 22, 31
Bessell, M. S., Castelli, F., & Plez, B. 1998, A&A, 333, 231
Borucki, W. J., Koch, D. G., Basri, G., et al. 2011, ApJ, 728, 117
Brown, T. M., Latham, D. W., Everett, M. E., & Esquerdo, G. A. 2011, AJ, 142, 112
Burke, C. J., McCullough, P. R., Valenti, J. A., et al. 2007, ApJ, 671, 2115
Creevey, O. L., Metcalfe, T. S., Brown, T. M., Jiménez-Reyes, S., & Belmonte, J. A. 2011, ApJ, 733, 38
Dean, J. F., Warren, P. R., & Cousins, A. W. J. 1978, MNRAS, 183, 569
De Gennaro, S., von Hippel, T., Jefferys, W. H., et al. 2009, ApJ, 696, 12
Demarque, P., Woo, J.-H., Kim, Y.-C., & Yi, S. K. 2004, ApJS, 155, 667
Ford, E. B. 2005, AJ, 129, 1706
Frinchaboy, P. M., & Majewski, S. R. 2008, AJ, 136, 118
Gallart, C., Zoccali, M., & Aparicio, A. 2005, ARA&A, 43, 387
Girardi, L., Williams, B. F., Gilbert, K. M., et al. 2010, ApJ, 724, 1030
Glushkova, E. V., Batyrshinova, V. M., & Ibragimov, M. A. 1999, AstL, 25, 86
Gregory, P. C. 2005, ApJ, 631, 1198
Hekker, S., Basu, S., Stello, D., et al. 2011, A&A, 530, 100
Huber, D., Bedding, T. R., Stello, D., et al. 2010, ApJ, 713, 109
Ivezić, Ž., Smith, J. A., Miknaitis, G., et al. 2007, in ASP Conf. Ser. 364, The Future of Photometric, Spectrophotometric and Polarimetric Standardization, ed. C. Sterken (San Francisco, CA: ASP), 165
Janes, K. A., & Heasley, J. N. 1993, PASP, 105, 527
Janes, K. A., & Hoq, S. 2011, AJ, 141, 92
Jester, S., Schneider, D. P., Richards, G. T., et al. 2005, AJ, 130, 873
Kallinger, T., Mosser, B., Hekker, S., et al. 2010, A&A, 522, 1
King, I. 1962, AJ, 67, 471
Landolt, A. U. 2009, AJ, 137, 4186
Lindoff, U. 1972, A&A, 16, 315

Luo, Y. P., Zhang, X. B., Luo, C. Q., Deng, L. C., & Luo, Z. Q. 2009, NewA, 14, 584
Majaess, D., Turner, D., & Lane, D. 2011, BAAS, 43, 322.08
Mamajek, E. E., Soderblom, D. R., & Wyse, R. F. G. (ed.) 2009, IAU Symp. 258, The Ages of Stars (Cambridge: Cambridge Univ. Press)
Marigo, P., Girardi, L., Bresson, A., et al. 2008, A&A, 482, 883
Meibom, S., Barnes, S. A., Latham, D. W., et al. 2011, ApJL, 733, L9
Meibom, S., & the Kepler Science Team. 2011, BAAS, 43, 311.03
Mermilliod, J.-C., & Mayor, M. 1990, A&A, 237, 61
Mills, E., Deliyannis, C., Sarajedini, A., & Platais, I. 2004, BAAS, 36, 1381
Monteiro, H., Dias, W. S., & Caetano, T. C. 2010, A&A, 516, A2
Perryman, M. A. C., Brown, A. G. A., Lebreton, Y., et al. 1998, A&A, 331, 81
Plummer, H. C. 1911, MNRAS, 71, 460
Press, W. H., Teukolsky, S. A., Vetterling, W. T., & Flannery, B. P. 2007, Numerical Recipes (Cambridge: Cambridge Univ. Press)
Rose, M. B., & Hintz, E. G. 2007, AJ, 134, 2067
Sanders, W. L. 1971, A&A, 15, 368
Schlegel, D. J., Finkbeiner, D. P., & Davis, M. 1998, ApJ, 500, 525
Soderblom, D. R. 2010, ARA&A, 48, 581
Stetson, P. B., Bruntt, H., & Grundahl, F. 2003, PASP, 115, 413
von Hippel, T., Jefferys, W. H., Scott, J., et al. 2006, ApJ, 645, 1436